Inner activation gate in S6 contributes to the state-dependent binding of cAMP in full-length HCN2 channel

Shengjun Wu, Weihua Gao, Changan Xie, Xinping Xu, Christina Vorvis, Farzana Marni, Amber R. Hackett, Qinglian Liu, and Lei Zhou

Department of Physiology and Biophysics, Virginia Commonwealth University School of Medicine, Richmond, VA 23298

Recently, applications of the patch-clamp fluorometry (PCF) technique in studies of cyclic nucleotide–gated (CNG) and hyperpolarization-activated, cyclic nucleotide–regulated (HCN) channels have provided direct evidence for the long-held notion that ligands preferably bind to and stabilize these channels in an open state. This state-dependent ligand–channel interaction involves contributions from not only the ligand-binding domain but also other discrete structural elements within the channel protein. This insight led us to investigate whether the pore of the HCN channel plays a role in the ligand–whole channel interaction. We used three well-characterized HCN channel blockers to probe the ion-conducting passage. The PCF technique was used to simultaneously monitor channel activity and cAMP binding. Two ionic blockers, Cs^+ and Mg^{2+}, effectively block channel conductance but have no obvious effect on cAMP binding. Surprisingly, ZD7288, an open channel blocker specific for HCN channels, significantly reduces the activity-dependent increase in cAMP binding. Independent biochemical assays exclude any nonspecific interaction between ZD7288 and isolated cAMP-binding domain. Because ZD7228 interacts with the inner pore region, where the activation gate is presumably located, we did an alanine scanning of the intracellular end of S6, from T426 to A435. Mutations of three residues, T426, M430, and H434, which are located at regular intervals on the S6 α-helix, enhance cAMP binding. In contrast, mutations of two residues in close proximity, F431A and I432A, dampen the response. Our results demonstrate that movements of the structural elements near the activation gate directly affect ligand binding affinity, which is a simple mechanistic explanation that could be applied to the interpretation of ligand gating in general.

INTRODUCTION

Ion channels mainly respond to two types of stimuli, voltage and ligand (Hille, 2001). Hyperpolarization-activated, cyclic nucleotide–regulated (HCN) channels, which are regulated by both of these stimuli, open upon membrane hyperpolarization and direct binding of intracellular cAMP molecules (Robinson and Siegelbaum, 2003; Craven and Zagotta, 2006; Biel et al., 2009). HCN channels belong to the superfamily of voltage-gated K channels and share a similar topology with CNG and EAG channels (Jan and Jan, 1990; Zagotta and Siegelbaum, 1996; Kaupp and Seifert, 2002). Each functional HCN channel contains four subunits. Within each subunit, there is a transmembrane domain (TMD) containing six transmembrane α-helixes (S1–S6). The S4 segment contains multiple positively charged residues and functions as the voltage sensor. However, in contrast to most other voltage-gated channels, the S4 segment of the HCN channel moves inward in response to membrane hyperpolarization during channel opening (Männikkö et al., 2002; Bell et al., 2004; Vemana et al., 2004). The ion-conducting pore is comprised of S5, S6, and the reentrant loop in between. The primary sequence of HCN channels in this region, especially the selectivity filter and S6, can be aligned perfectly to the sequences from other potassium channels without gaps. Downstream from the selectivity filter, S6 segments from the four subunits assemble together and form the ion-conducting passage. Similar to other K channels, the S6 segment in the HCN channel harbors an activation gate that moves during channel gating and controls the ionic flow (Hackos et al., 2002; Rothberg et al., 2003; Shin et al., 2004; Webster et al., 2004; Swartz, 2005).

On the intracellular side, HCN channels contain a canonical cyclic nucleotide–binding domain (CNBD), homologous to the CNBD found in other proteins such as cAMP-dependent protein kinase (PKA), cGMP-dependent protein kinase (PKG), and CNG channels. Intracellular cAMP molecules directly bind to the CNBD and open the channel. cAMP-dependent gating increases

S. Wu and W. Gao contributed equally to this paper.
Correspondence to Lei Zhou: lzhou@vcu.edu

S. Wu's present address is Dept. of Psychology, School of Aerospace Medicine, Fourth Military Medical University, Xi'an, Shaanxi 710032, China.

Abbreviations used in this paper: CL, C-linker; CNBD, cyclic nucleotide–binding domain; HCN, hyperpolarization activated, cyclic nucleotide regulated; ITC, isothermal titration calorimetry; mHCN2, mouse HCN2; PCF, patch-clamp fluorometry; TMD, transmembrane domain; WT, wild type.

The Rockefeller University Press $30.00
J. Gen. Physiol. Vol. 140 No. 1 29–39
www.jgp.org/cgi/doi/10.1085/jgp.201110749

the macroscopic current amplitude, shifts the channel activation toward less hyperpolarizing potentials, speeds up channel activation, and slows down channel deactivation. So, how does cAMP binding trigger a series of molecular events that result in the gate opening? Functional assays performed on the full-length HCN channel as well as biochemical assays on purified C-terminal fragments, including the C-linker (CL; the 90-aa peptide downstream from S6) and the CNBD, support a transition in the molecular symmetry from a dimer-of-dimer to a gating ring–like tetrameric structure (Ulens and Siegelbaum, 2003; Zagotta et al., 2003; Rosenbaum and Gordon, 2004). The crystal structure of the CL-CNBD fragment, which forms the core of the cAMP-dependent gating machinery in both CNG and HCN channels, has been published for mouse HCN2 (mHCN2), sea urchin HCN, and human HCN4 channels (Zagotta et al., 2003; Flynn et al., 2007; Xu et al., 2010). These crystal structures provide an atomic view over the local cAMP–CNBD interactions and the assembly of the four subunits but limited information regarding the coupling between cAMP binding and channel opening.

The cAMP-dependent gating observed in HCN channels can be categorized within the realm of protein allostery, a research theme broadly applied to not only ligand-gated channels and receptors but also other types of macromolecules such as protein enzymes. Two general models for protein allostery exist: the induced fit model and the preexisting equilibrium model. The preexisting equilibrium model, also known as the conformation selective model, postulates that proteins in either the resting or active state coexist. Although ligands are able to interact with the protein in either state, they preferably bind to the protein in the active state, which shifts the equilibrium from resting to active (Richards and Gordon, 2000; Altomare et al., 2001; Wang et al., 2002; Zhou et al., 2004; Biskup et al., 2007; Zhou and Siegelbaum, 2007). A similar cyclic allosteric gating scheme exists for ligand-gated ion channels; however, collecting the direct evidence had been difficult, mainly because of the technical challenges involved in specific measurement of ligand binding affinity at a particular functional state. With the advent of fluorescently labeled ligands, the patch-clamp fluorometry (PCF) technique made simultaneous measurements of ligand binding and channel activity feasible and has been successfully applied to the study of CNG and HCN channels (Biskup et al., 2007; Kusch et al., 2010; Wu et al., 2011). PCF results clearly demonstrate that cAMP binds to the channels in the closed state and, more importantly, binds to the channels in the open state with greater affinity. Potentially, this model of state-dependent ligand binding can be applied as a general principle for ligand gating, but resolving the corresponding structural basis remains a daunting task.

In this study, we aim to address which discrete elements in the HCN channel contribute to the state-dependent interaction between cAMP and whole channel protein. We started from the channel pore and used three well-characterized HCN channel blockers to probe the elements along the ion-conducting passage. Two ionic pore blockers, Cs^+ and Mg^{2+}, have no effect. However, an open channel blocker, ZD7288, significantly reduces the activation-dependent increase in cAMP binding. Following this lead, we performed an alanine scanning of the intracellular end of S6 and identified multiple mutations that affect cAMP binding. These results illustrate an intriguing communication between the channel activation gate and the ligand-binding domain, which are ~50 Å apart.

MATERIALS AND METHODS

PCF

Xenopus laevis oocytes were used for heterologously expressing mHCN2 channels. cDNA of the mHCN2 channel in the pGH vector was provided by S. Siegelbaum (Columbia University, New York, NY). 50 ng of in vitro transcribed cRNAs was injected into each oocyte. After 2–4 d of incubation at 17°C, injected oocytes expressed a sufficient amount of HCN channels to allow for detection. All of the following experiments were performed at room temperature. For PCF measurements, ionic currents and optical signals were collected from the membrane patch within the glass pipette in the inside-out configuration. The standard recording solution contained 110 mM KCl, 1 mM $MgCl_2$, 1 mM EGTA, and 5 mM HEPES, pH 7.4 (adjusted with KOH). The pipette solution and bath profusion solution are symmetrical. Zero Mg^{2+} solution contained 110 mM KCl, 1 mM $MgCl_2$, 1 mM EGTA, 1.5 mM EDTA, and 5 mM HEPES, pH 7.4. High Mg^{2+} solution contained 110 mM KCl, 6 mM $MgCl_2$, 1 mM EGTA, and 5 mM HEPES, pH 7.4.

The PCF setups were constructed using a microscope (BX50WI; Olympus) equipped with a 60× water immersion lens (LUMPlanFL). A 473-nm DPSS (diode-pumped solid-state) laser was used as the excitation light source. The following filter set was used for collecting NBD fluorescence: exciter, D480/30; dichroic mirror, DC505LP; emitter, D510LP. Optical signals were detected by an electron-multiplying charge-coupled device camera (Cascade 1K; Photometrics) and analyzed using ImageJ software (National Institutes of Health). A DAQ board (National Instruments) was used for converting analogue and digital I/O. The laser light source, the charge-coupled device camera exposure, and the amplifier for patch-clamp recording were synchronized by TTL (transistor–transistor logic) signals. The TurboReg program was used for image alignment. For measuring the fluorescence signal specific to excised membrane, a region of interest was selected around the arc of membrane patch in the recording pipette. ΔF was defined as the mean fluorescence intensity in the region of interest with the background fluorescence subtracted. The ΔF value collected at the holding potential of −40 mV (ΔF_{-40mV}), corresponding to the binding of cAMP to the channels at a closed state, was used as a reference to normalize the activity-dependent fluorescence signals collected along a voltage step ($\Delta\Delta F$). The fluorescent cAMP analogue, 8-NBD-cAMP, was obtained from Biolog.

Biochemical binding assays on purified mHCN2 C-terminal protein

The DNA fragment containing the CL and the CNBD of mHCN2 channel (D443 to H645) was cloned into the pSMT3 vector and

expressed in *Escherichia coli* BL21 cells. A standard three-step purification scheme, including Ni affinity chromatography, ion exchange chromatography, and size exclusion chromatography, was used to purify mHCN2 protein. After eluting from the Ni-NTA column, the protein sample was incubated with Ulp1 protease to remove the His-Smt3 tag. After the last purification step, purified protein sample was concentrated to 10 mg/ml and flash frozen in liquid nitrogen. Before performing the biochemical binding assays, protein samples were extensively dialyzed to remove any residual bound cAMP molecules. Isothermal titration calorimetry (ITC; iTC200 microcalorimeter; MicroCal, Inc.) was used to measure the binding of cAMP to 100 µM of purified mHCN2 protein. All ITC measurements were performed at 37°C. The excitation and emission spectra of 5 µM 8-NBD-cAMP in complex with 20 µM of purified mHCN2 protein was measured by a photon-counting spectrofluorometer (PC1; ISS, Inc.).

Online supplemental material

Fig. S1 shows experimental data on ZD7288's effects on channel conductance and cAMP binding in the presence of Mg^{2+}. Fig. S2 shows an ITC assay on the interaction between ZD7288 and the CL-CNBD fragment; the ITC results of cAMP binding to the CL-CNBD fragment are shown as positive control. Fig. S3 shows the sequence alignment for pore S6 regions from HCN, CNG, and other K channels. Fig. S4 shows the structural modeling results based on KcsA and MthK structures. Online supplemental material is available at http://www.jgp.org/cgi/content/full/jgp.201110749/DC1.

RESULTS

Cs^+ and Mg^{2+} block ionic conductance but have no effects on cAMP binding

Previous research has established that the interaction between cAMP and the full-length HCN channel is dynamic and depends on the channel's functional state (Kusch et al., 2010; Wu et al., 2011). This state-dependent ligand–channel interaction should be the result of a concerted action by discrete structural elements. We first studied the ion-conducting pore and separately tested three well-characterized HCN channels blockers, Cs^+, Mg^{2+}, and ZD7288 (Fig. 1 A). Ionic current and cAMP binding were simultaneously monitored by the PCF technique, with 8-NBD-cAMP being used as a fluorescent indicator for cAMP binding. Previous biochemical

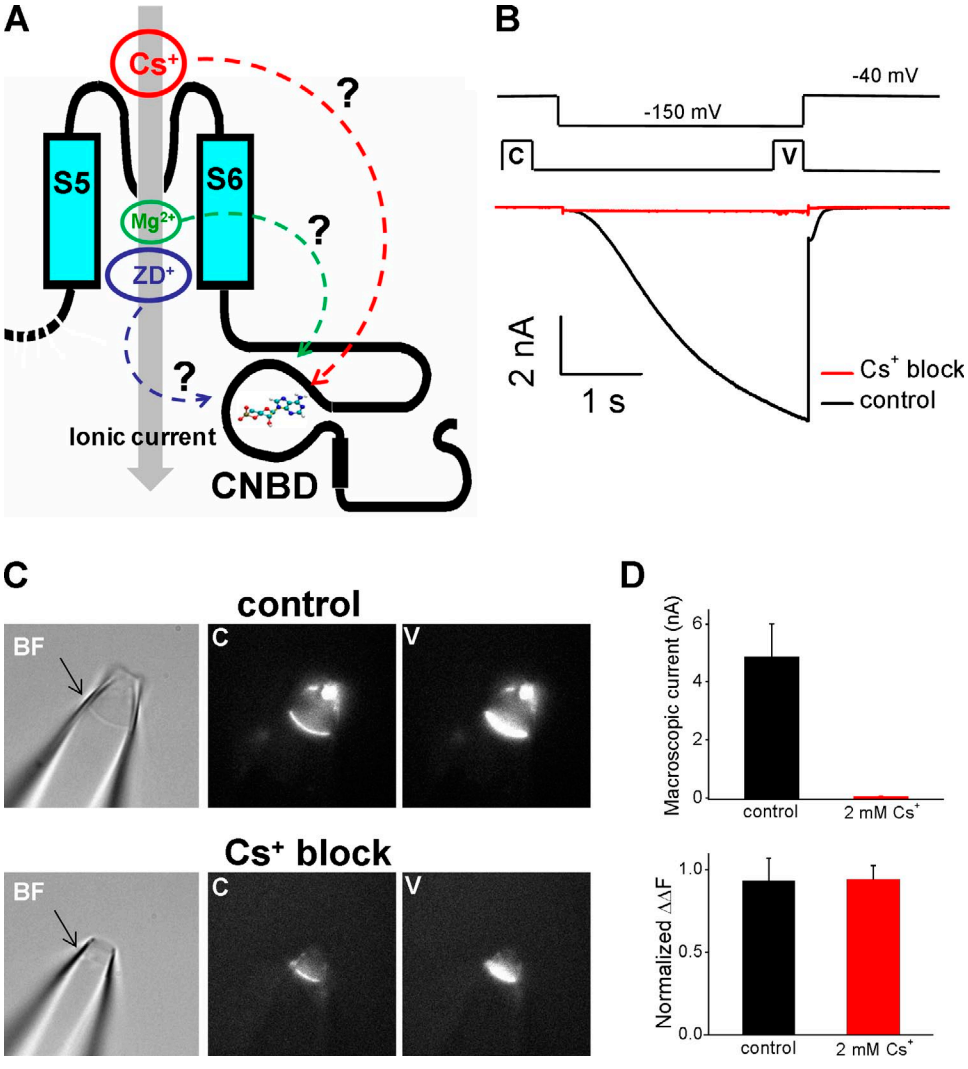

Figure 1. Extracellular Cs^+ blocks the ionic conductance but has no effect on cAMP binding. (A) A schematic model showing the pore region and the CNBD in HCN channels. (B) Voltage protocol (top), timing of image collection (middle), and ionic current traces (bottom). The black line indicates control condition without Cs^+; the red indicates 2 mM Cs^+ added to the pipette (extracellular) solution. (C) Brightfield (BF) images of the membrane patch (indicated by arrows) and the corresponding fluorescence images collected before (C) or near the end of the hyperpolarizing voltage step (V). (D) Comparison of current amplitude (top) and fluorescence intensity (bottom) between control (black) and with Cs^+ (red) in the pipette solution. The difference in the current amplitude between control and Cs^+ was significant (independent samples t test: $t = 3.57$, $P < 0.01$). No significant difference in the fluorescence intensity was found (independent samples t test: $t = 0.05$, $P = 0.96$). Error bars indicate standard error.

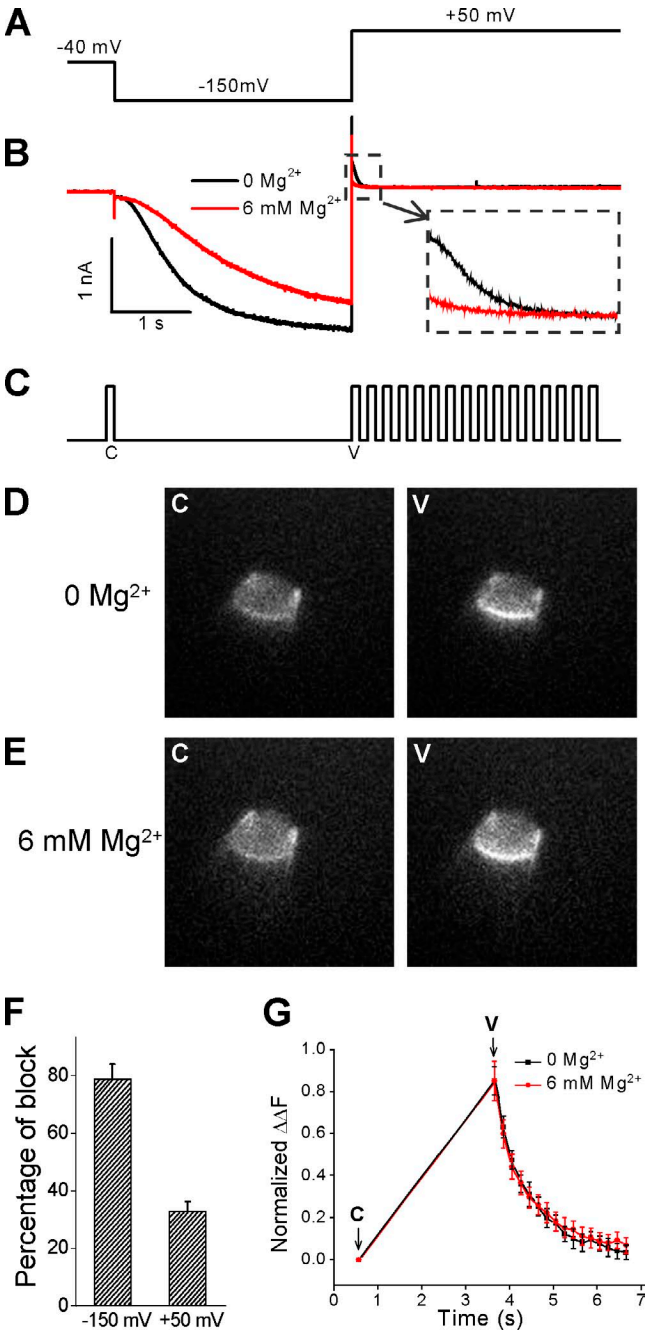

Figure 2. Intracellular Mg^{2+} blocks the ionic conductance but has no effect on cAMP binding. (A) A hyperpolarizing voltage step was used to activate the channel. Tail current was measured at 50 mV. (B) The corresponding current trace with no Mg^{2+} or 6 mM Mg^{2+}. The inset shows an expanded view of the tail currents. (C) TTL signals from the charge-coupled device camera exposure port showing the timing of image collections. A series of images were collected before the voltage step (C, cAMP binding to the channels in the closed/resting state), immediately after the voltage step (V, maximal cAMP binding to channels in the open state), and during channel deactivation. (D) Raw fluorescence images collected before (C) and immediately after the voltage step (V) without Mg^{2+} in the bath solution. (E) Fluorescence images collected with 6 mM Mg^{2+} in the bath. (F) Mg^{2+} significantly inhibited both the inward macroscopic current (left, recorded at −150 mV) and outward tail current (right, recorded at 50 mV; independent samples *t* test: $t = 6.74$, $P < 0.01$). (G) Time course of fluorescence intensity changes without Mg^{2+} or with 6 mM Mg^{2+} in the bath. No significant difference was found (independent samples *t* test results at 3.65 s: $t = 0.11$, $P = 0.99$). (F and G) Error bars indicate standard error.

and electrophysiological characterizations have established that 8-NBD-cAMP binds to and regulates the HCN channel in a manner similar to cAMP (Wu et al., 2011).

We started with Cs^+, which blocks HCN channel from the extracellular side (Fain et al., 1978; Barnes and Hille, 1989). Extracellular Cs^+ interacts with residues either on the extracellular side of the pore or deep in the selectivity filter (DiFrancesco, 1982; Denyer and Brown, 1990). Because the membrane patch in the recording pipette was in the inside-out configuration, we added 2 mM Cs^+ to the pipette solution and 0.1 µM 8-NBD-cAMP to the bath solution. The membrane potential was held at −40 mV, and a hyperpolarizing voltage step of −150 mV was used to activate the channel (Fig. 1 B). Two images were collected before (C) and near the end of the voltage step (V). Under the control condition (without Cs^+), a significant increase in ligand binding was observed along with channel activation (Fig. 1 C, top). With 2 mM Cs^+, the inward ionic current was completely abolished. Impressively, the activity-dependent increase in cAMP binding remained the same (Fig. 1, C [bottom] and D). Thus, extracellular Cs^+ separates the ionic conductance from the activity-dependent increase in cAMP binding. These data suggest that the passage of ions through the conducting pore is not a prerequisite for the dynamic interaction between cAMP and the functional full-length channel. To a certain degree, the optical detection of ligand binding in the absence of an ion-conducting pore is reminiscent of the electrical isolation of the gating charge movement for voltage-gated channels. Both approaches provide quantitative measurements of the stimuli that initiate channel gating.

Next we tested Mg^{2+}, a divalent ion that blocks HCN channels from the intracellular side (Lyashchenko and Tibbs, 2008; Vemana et al., 2008). The Mg^{2+}-interacting site has been mapped to the cysteine residue in the CIGYG signature sequence within the HCN channel selectivity filter (Vemana et al., 2008). Mutating this cysteine to serine or threonine significantly reduces the affinity to Mg^{2+}. To monitor the inhibition of outward current by intracellular Mg^{2+}, we measured the outward tail current at a holding potential of 50 mV (Fig. 2 A). Adding 6 mM Mg^{2+} slightly reduced the inward current but almost completely blocked the outward conductance (Fig. 2 B, red trace; summary in Fig. 2 F). Simultaneously, we measured the cAMP binding using a 17-image protocol. Similar to the observation with Cs^+, the activity-dependent cAMP binding was largely preserved (Fig. 2, D and E; summary in Fig. 2 G).

These experiments support that blocking the ionic conductance, either from the extracellular side by Cs^+ or from the intracellular side by Mg^{2+}, has no direct effect on cAMP binding. Molecular elements close to the selectivity filter in the pore most likely do not contribute to the state-dependent cAMP binding in the full-length HCN channel.

ZD7288 blocks channel conductance and also reduces dynamic cAMP binding

Next, we asked whether other molecular elements in the pore, especially the activation gate near the intracellular end of S6, play a role in cAMP binding. We tested ZD7288, an open channel blocker which is specific for HCN channels (BoSmith et al., 1993). The interacting site has been mapped to the intracellular end of S6, where the activation gate is presumably located (Rothberg et al., 2002; Shin et al., 2004). ZD7288 carries a unit of positive charge but is an organic molecule with a molecular weight of 293, making it different from Cs^+ and Mg^{2+} in both the binding site and the blocking mechanism. We applied ZD7288 at a concentration of up to 100 µM and observed a moderate reduction in cAMP binding (Fig. S1). To magnify the blocking effects, we tested a hypothesis that had been surprisingly overlooked by previous studies. Because both ZD7288 and Mg^{2+} interact with the inner pore region and carry positive charges, they may compete with each other in blocking the HCN channel. To test this possibility, we increased the amount of EDTA in our solution to reduce

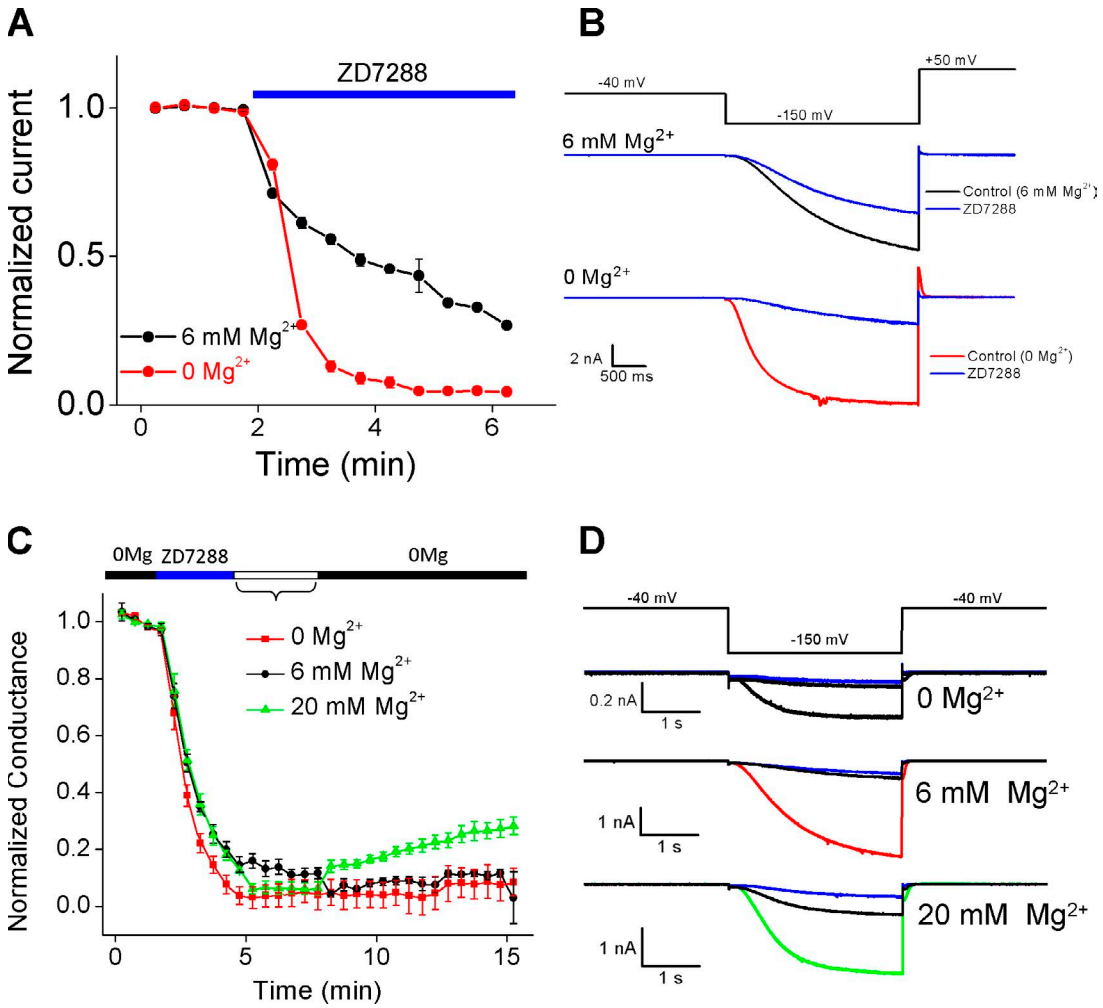

Figure 3. Intracellular Mg^{2+} reduces the efficacy of ZD7288 in blocking HCN channel conductance. (A) Macroscopic currents blocked by 100 µM ZD7288 (application indicated by the blue bar). The black line indicates 6 mM Mg^{2+} added in the bath solution; the red line indicates 0 Mg^{2+}. The difference between 0 Mg^{2+} and 6 Mg^{2+} at time 255 s is statistically significant (independent samples *t* test: $t = 13.85$, $P < 0.01$). (B, top) Voltage protocol used. (middle) Current traces recorded with 6 mM Mg^{2+} in the bath solution. (bottom) 0 Mg^{2+}. Current traces recorded with ZD7288 are shown in blue. Control traces without ZD7288 are shown in either black (6 mM Mg^{2+}) or red (0 Mg^{2+}). (C) Washing off the ZD7288 block (blue bar) by exposing the membrane patch to different concentrations of Mg^{2+} (open bar). The red line indicates without Mg^{2+}; the black line indicates 6 mM Mg^{2+}; the green line indicates 20 mM Mg^{2+}. Recovery of HCN current was tested in the absence of Mg^{2+}. (A and C) Error bars indicate standard error. (D) Corresponding voltage protocol and representative current traces.

the free Mg^{2+} concentration. Without Mg^{2+}, the blockade of ionic current by ZD7288 was faster and more complete (Fig. 3, A and B). Similarly, the wash off of ZD7288 block was also affected by Mg^{2+}, as exposing the membrane patch to 20 mM Mg^{2+} significantly improved the recovery of channel conductance (Fig. 3, C and D). These results clearly demonstrate the competition between Mg^{2+} and ZD7288 in blocking HCN channel conductance.

Next, we tested whether the binding of cAMP in the presence of ZD7288 would be different in the absence of Mg^{2+}. We used the same voltage protocol to activate the channel but two separate optical recording schemes during channel activation (Fig. 4 A) or deactivation (Fig. 4 B). In contrast to the condition with Mg^{2+} where only a moderate effect was observed, ZD7288 reduced the maximal cAMP binding by nearly 40% in the absence of Mg^{2+} (Fig. 4, C–F). To determine whether ZD7288 directly binds to or interferes with the local interaction between cAMP and isolated CNBD fragment, we performed biochemical assays on purified mHCN2 CL-CNBD fragments. As expected, using ZD7288 at a concentration up to 300 μM had no effect on the fluorescence spectra of 8-NBD-cAMP or the binding of cAMP to the purified mHCN2 C-terminal protein (Fig. 5, A and B). We also did ITC experiments and

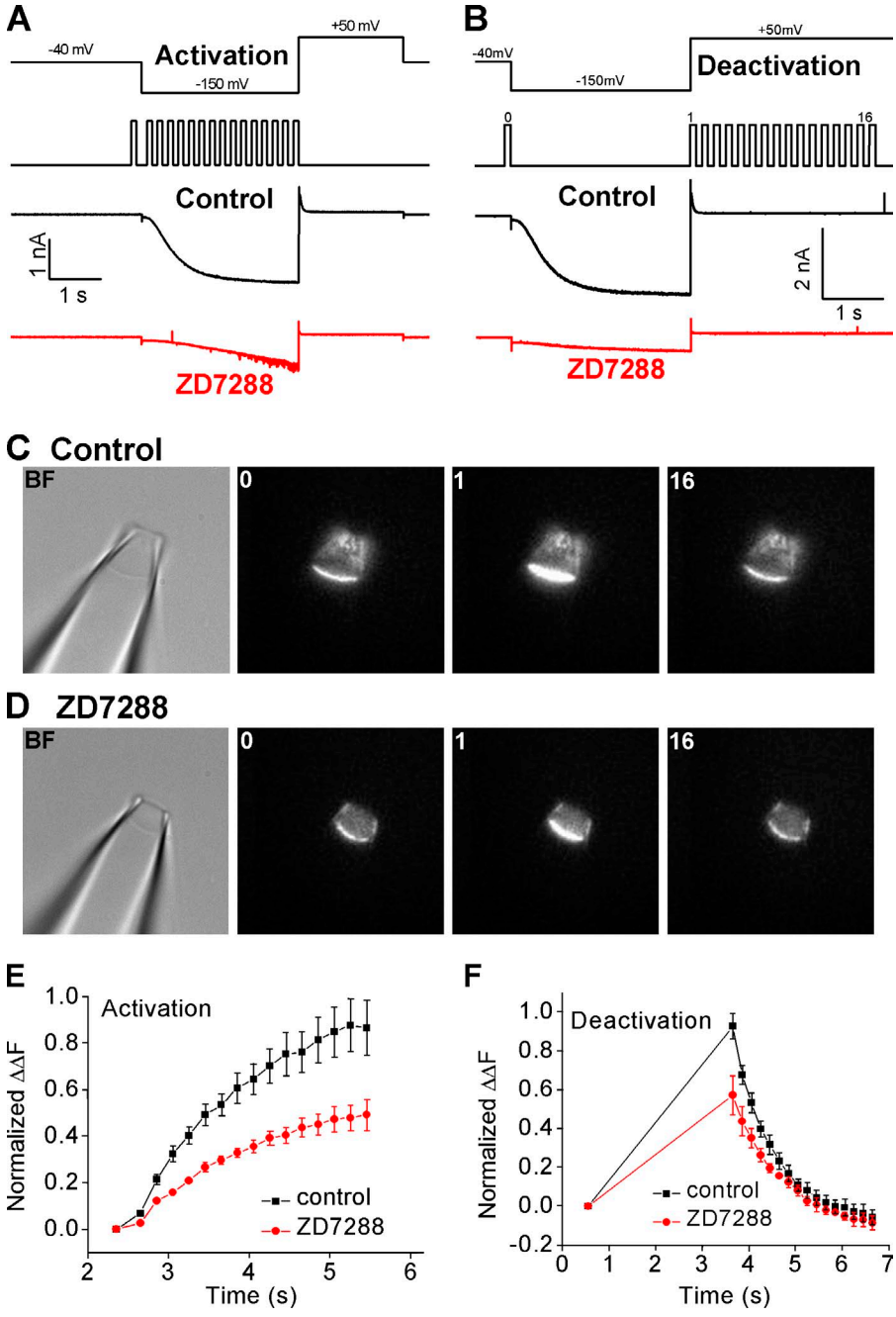

Figure 4. ZD7288 blocks ionic conductance and reduces activity-dependent cAMP binding. (A, top) Voltage protocol used for channel activation (−150 mV) and tail current recording (50 mV). (middle) Time course of image collection. (bottom) Current traces of control (black) and with 100 μM ZD7288 (red). (B) The same experimental protocol used as in A except fluorescence images were collected during channel deactivation (50 mV). (C) Brightfield (BF) image of the patch pipette and fluorescence images collected before (0), at the beginning (1), and near the end (16) of channel deactivation. Control without ZD7288. (D) Brightfield and fluorescence images collected during channel deactivation with ZD7288 added in the bath solution. (E) Normalized fluorescence intensity change during channel activation. The fluorescence intensity measured from image 0 was used as a reference. The black line indicates control; the red line indicates 100 μM ZD7288. At 5.45 s, the difference between control and ZD7288 was significant (independent samples *t* test: $t = 2.46$, $P < 0.05$). (F) Normalized fluorescence intensity change during channel deactivation. The black line indicates control; the red line indicates 100 μM ZD7288. At 3.65 s, the difference between control and ZD7288 was significant (independent samples *t* test: $t = 2.96$, $P < 0.05$). Because of photobleaching, the fluorescence intensity measured near the end of the time course was slightly lower than that at the beginning. (E and F) Error bars indicate standard error.

confirmed that ZD7288 had no direct interaction with isolated CL-CNBD (Fig. S2). Together with the aforementioned PCF results, it is clear that ZD7288, an open channel blocker in close contact with the activation gate in S6, blocks the ionic conductance and allosterically reduces cAMP binding. Given the distance between the inner pore region and the core in the CNBD, these observations indicate a direct contribution by the activation gate or the nearby residues to the state-dependent cAMP binding in the full-length channel. Furthermore, these results manifest the absolute necessity of interpreting ligand gating at global, whole channel protein level.

Residues near the activation gate in S6 contribute to dynamic cAMP binding

To strengthen the connection between the inner pore and the dynamic cAMP binding, we did an alanine scanning of the intracellular end of S6, from T426 to A435 (Fig. 6 A). Among them, two residues, M430 and I432, have been shown to interact with ZD7288 (Cheng et al., 2007; Chan et al., 2009). Each of the alanine mutant channels were characterized by PCF. In the wild-type (WT) mHCN2 channel, near the peak of channel activation, the dynamic cAMP binding (ΔΔF) was almost doubled (199 ± 12%) when compared with the resting level measured at −40mV (ΔF_{-40mV}). Among the nine alanine replacement mutant channels tested, the activity-dependent cAMP binding was affected in several of them (Fig. 6, B–D). In the H434A mutant channel, although no obvious change in ionic current was detected, the ΔΔF was increased by almost threefold (388 ± 35%). In contrast, the I432A mutation reduced the maximal cAMP binding to 128 ± 4%, which is significantly lower than that of the WT channel. Moreover, the I432A mutation clearly separates the kinetics of channel opening from that of cAMP binding. This is a novel observation because all previous PCF studies on either CNG or HCN channels show a close correlation between channel activation and ligand binding (Biskup et al., 2007; Kusch et al., 2010; Wu et al., 2011). Collectively, these mutagenesis experiments are particularly relevant because they directly link the structural elements near the activation gate in S6 to the ligand binding in whole channel protein.

Next, we sought to determine whether a pattern could be identified based on the PCF results for the nine mutations (Fig. 6 E). Interestingly, the three alanine mutations that enhanced cAMP binding, T426A, M430A, and H434A, are distributed at regular intervals on S6 and form a cluster on one side of the α-helix. In contrast, the two mutations that dampened cAMP binding, F431A and I432A, are located in proximity but on the opposite side of the α-helix. These results prompted us to look for the location of these residues in S6. We used the Kv1.2 crystal structure as a template to model the S5-pore-S6 region of mHCN2 channel (Fig. 6 A and Fig. S3). As illustrated in the HCN S5-pore-S6 model, the side chains of T426, M430, and H434 point toward the S6 segment of a neighboring subunit, whereas the side chain of I432 is in contact with the S6 from another neighboring subunit (Fig. 6 F). We also used representative bacterial potassium structures that are presumably in either closed (KcsA) or open (MthK) state as templates for modeling (Fig. S4). However, without additional experimental evidence, excavating the corresponding structural details would be difficult. Nevertheless, in conjunction with the aforementioned experimental results, these experiments suggest that

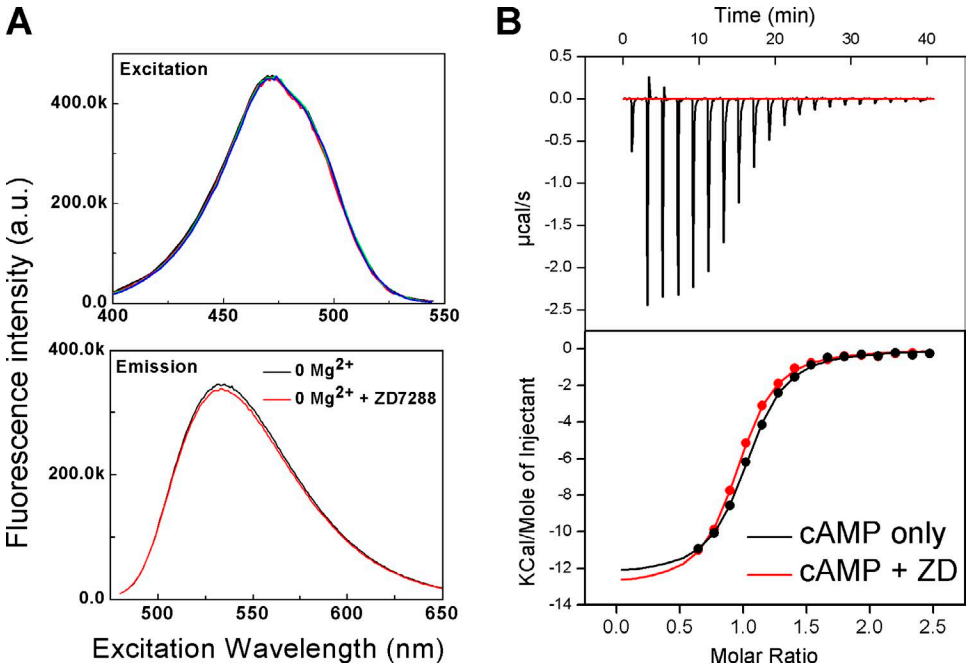

Figure 5. Biochemical assays exclude the possibility of direct contact between ZD7288 and the CL-CNBD fragment and the interference with cAMP binding. (A) ZD7288 has no effect on the excitation (top) and emission (bottom) spectra of 8-NBD-cAMP in complex with purified HCN channel C-terminal protein. The effect of Mg^{2+} was tested separately, and no difference was found between 0 and 6 mM Mg^{2+}. (B) ITC results showing that ZD7288 does not interfere with normal cAMP binding. (top) Raw trace showing the rate of heat exchange versus the time of cAMP injection (with 300 µM ZD7288). (bottom) Binding curves of cAMP to mHCN2 protein in the absence (black) and presence (red) of ZD7288.

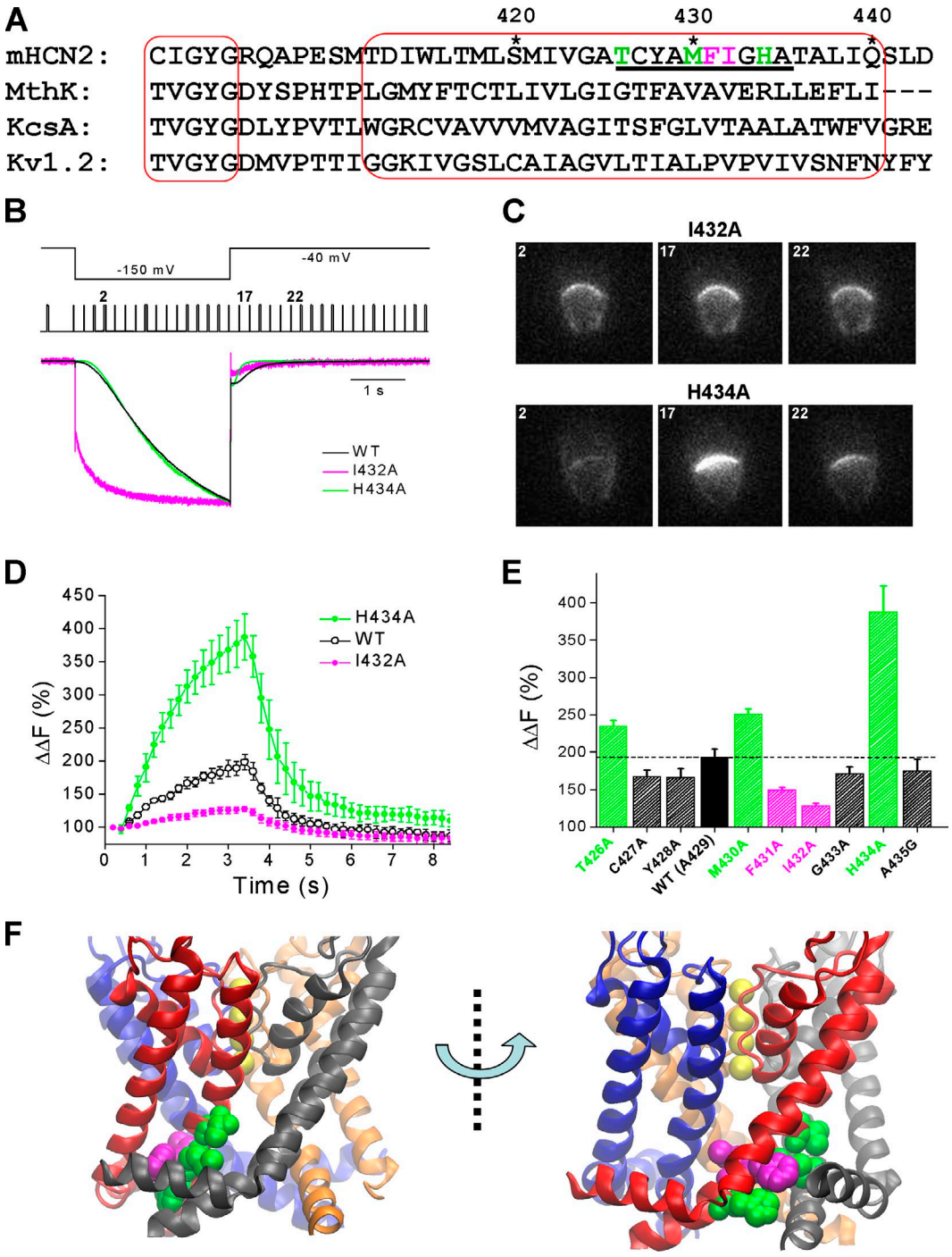

Figure 6. Alanine scanning of residues near the intracellular end of S6. (A) Alignment of primary sequences from mHCN2, MthK, KcsA, and Kv1.2 channels. Selectivity filter and S6 segment are indicated by red squares. Numbers on the top refer to the residue positions in mHCN2. Asterisks indicate the sequence number for the mHCN2 channel. Underlining indicates the region scanned by alanine replacement. Green and magenta letters indicate that the corresponding alanine replacements either increase (green) or decrease (magenta) the dynamic cAMP binding. (B) Normalized macroscopic current traces for WT (black), mHCN2/I432A (magenta), and mHCN2/H434A (green) channels. Voltage step and timing of fluorescent image collection are shown on top of the current traces. (C) Representative fluorescence images for I432A and H434A mutant channels. Timing of fluorescence image collection is shown in B. (D) Profiles of cAMP binding in response to a hyperpolarizing voltage step for WT mHCN2 (black), mHCN2/I432A (magenta), and mHCN2/H434A (green) channels. Fluorescence intensities are normalized to the value collected at −40 mV. (E) Summary of the PCF results. The mHCN2 channel contains two endogenous alanine residues in this region, A429 and A435. A435 was tested by a glycine replacement. A429 was not tested so the result represents the WT channel value. Independent samples *t* test shows that each of the following alanine mutants, T426A, M430A, F431A, I432A, and H434A, are significantly different from WT (A429; $P < 0.01$). (D and E) Error bars indicate standard error. (F) Structure model of the S5-pore-S6 region from the mHCN2 channel. The crystal structure of Kv1.2/2.1

corresponding to channel activation, movements of the gate or the elements near S6 are directly coupled to the ligand sensitivity in the full-length channel. These results provide a simple but reasonable interpretation of the implementation of cAMP-dependent gating in the HCN channel.

DISCUSSION

Mainly relying on the technique of PCF, recent studies on cAMP-gated CNG and HCN channels provide direct evidence supporting the long-held notion that ligands bind to the channels in open state at a higher affinity and thus stabilize the open state (Biskup et al., 2007; Kusch et al., 2010; Wu et al., 2011). The primary goal of the current study was to determine the contributions to state-dependent cAMP binding by discrete subdomains within the full-length channel. Starting at the ion-conducting pore, we used three classical HCN blockers. Different from two ionic blockers that effectively block the ionic conductance but have no effect on cAMP binding, ZD7288, an open channel blocker for HCN channels, significantly reduces the activity-dependent cAMP binding. Further alanine scanning experiments confirmed the involvement of the intracellular end of S6, presumably where the inner activation gate is located.

Our mutagenesis experiments establish the essential connection between the movements of the inner pore and the cAMP binding to the CNBD. Among the nine residues tested, I432A mutation has the strongest effect in dampening the increase in cAMP binding upon channel activation. Interestingly, the location of I432 in mHCN2 corresponds to the middle residue in the PXP motif of Kv channels, which generates a kink near the intracellular end of S6 and has profound effects on the gating of Kv channels. The residue between two prolines could be valine (in most Kv channels, HCN1) or isoleucine (in Kv2.1, HCN2–4). In HCN channels, multiple lines of evidence suggest that this location critically affects both voltage- and cAMP-dependent gatings. I432 in HCN2 or the corresponding V379 in HCN1 has a strong interaction with ZD7288. The corresponding Alanine replacement mutations significantly affect the opening rate in response to membrane hyperpolarization (Cheng et al., 2007; Chan et al., 2009). In our PCF experiments, the I432A mutation clearly separates channel opening and cAMP binding: channel opening becomes much faster, but cAMP binding is severely dampened. This is significant because previously published PCF studies show slightly different but closely matched profiles of the two processes (Biskup et al., 2007; Kusch et al., 2010; Wu et al., 2011). It is possible that I432 as well as nearby residues play a pivotal role in integrating two gating processes and balance the energetic input from voltage sensor movement and cAMP binding. Because of unknown mechanisms, the I432A mutation disrupts this balance and favors the voltage-dependent channel opening.

It remains to be determined how H434A leads to such a dramatic increase (about fourfold) in the activity-dependent cAMP binding. Given the locations of I432 and H434, situated on opposite sides of the S6 α-helix, a rotational motion in S6 might occur during channel opening. So, how does the movement of the activation gate influence cAMP binding that occurs distantly? The structural elements located in between should play important roles. One possible candidate is the CL region between S6 and CNBD that has been repeatedly shown to be critical for the efficacy of ligand gating in both the CNG and HCN channels (Zong et al., 1998; Paoletti et al., 1999; Craven and Zagotta, 2004; Zhou et al., 2004; Hua and Gordon, 2005). Moreover, the CL is in direct contact with the S4–S5 linker in the TMD, which is another possible candidate mediating the allosteric couplings. The interaction between the S4–S5 linker and the CL has been studied in various types of channels (Chen et al., 2001; Decher et al., 2004; Prole and Yellen, 2006). Based on the TMD structure of the Kv channel and the HCN channel C-terminal structure, the S4–S5 linker should be in close proximity of the first α-helix in the CL. Further studies are needed to clarify the synergistic actions that involve each structural element in this critical region: the S4–S5 linker, the CL, and the activation gate.

The aforementioned PCF results suggest that the functioning state of the HCN channel critically determines its binding affinity to intracellular cAMP molecules. This actually explains an observation that has been puzzling since the discovery of ZD7288 decades ago. In the whole cell preparation, ZD7288 blocks the ionic conductance but at the same time induces a negative shift in the voltage-dependent channel activation (Harris and Constanti, 1995). Based on the aforementioned results, ZD7288 does not simply block the ionic current but also significantly reduces cAMP binding, which explains the negative shift in the presence of ZD7288 and physiological concentration of cAMP. Noticeably, many other HCN channel blockers, including Ivabradine, a clinically approved drug for reducing heart rate, share similar binding sites and blocking mechanisms with ZD7288. It would be interesting to study whether those HCN channel blockers also have an effect

chimera (Protein Data Bank accession no. 2R9R; Long et al., 2007) was used as the template for modeling. Side chains of T426, M430, and H434, of which the corresponding alanine replacement mutations increased cAMP binding, are shown in green. Side chains of F431 and I432, of which the alanine replacement mutations reduced cAMP binding, are shown in magenta.

on the binding affinity to cAMP. Furthermore, the competition between ZD7288 and Mg^{2+} in binding to and blocking the HCN channel is a surprising observation. In Kv channels, Mg^{2+} interferes with the binding of positively charged small organic compounds such as spermine to the inner pore (Lopatin et al., 1994; Yang et al., 1995). Our results raise the possibility that intracellular Mg^{2+} at the millimolar range may have a direct effect on compounds that target the inner pore region in HCN channels.

The mechanism by which ligands bind to and allosterically regulate protein function continues to be a central theme in the biophysical study of proteins, including enzymes and ion channels (Monod et al., 1965; Changeux and Edelstein, 2005; Henzler-Wildman et al., 2007). It remains an intriguing question as to how the ligand binding site cross talks with the activation site at which protein fulfills its function. The unique biophysical properties of the HCN channel, which is dually regulated by voltage and ligands, make it an ideal research target. Following the observation that ligands open the channel by specifically binding to and stabilizing the channels in the open state, we went one step further to show that the inner activation gate is directly involved in the state-dependent ligand–channel interaction. Our experiments shed light on not only the molecular mechanism of the cAMP-dependent gating in the HCN channel but also the implementation of protein allostery in other ligand-gated channels and receptors.

We thank Drs. L. De Felice, D. Logothetis, and G. Tseng for their insightful comments and suggestions on this manuscript and the technical support from S. Gruszecki, S. Shrestha, and H. Vaananen.

This work was supported by the startup funds from the Virginia Commonwealth University and American Heart Association Grant-in-Aid (11BGIA7850004) to L. Zhou and Q. Liu.

Sharona E. Gordon served as editor.

Submitted: 30 November 2011
Accepted: 23 May 2012

REFERENCES

Altomare, C., A. Bucchi, E. Camatini, M. Baruscotti, C. Viscomi, A. Moroni, and D. DiFrancesco. 2001. Integrated allosteric model of voltage gating of HCN channels. *J. Gen. Physiol.* 117:519–532. http://dx.doi.org/10.1085/jgp.117.6.519

Barnes, S., and B. Hille. 1989. Ionic channels of the inner segment of tiger salamander cone photoreceptors. *J. Gen. Physiol.* 94:719–743. http://dx.doi.org/10.1085/jgp.94.4.719

Bell, D.C., H. Yao, R.C. Saenger, J.H. Riley, and S.A. Siegelbaum. 2004. Changes in local S4 environment provide a voltage-sensing mechanism for mammalian hyperpolarization–activated HCN channels. *J. Gen. Physiol.* 123:5–19. http://dx.doi.org/10.1085/jgp.200308918

Biel, M., C. Wahl-Schott, S. Michalakis, and X. Zong. 2009. Hyperpolarization-activated cation channels: from genes to function. *Physiol. Rev.* 89:847–885. http://dx.doi.org/10.1152/physrev.00029.2008

Biskup, C., J. Kusch, E. Schulz, V. Nache, F. Schwede, F. Lehmann, V. Hagen, and K. Benndorf. 2007. Relating ligand binding to activation gating in CNGA2 channels. *Nature.* 446:440–443. http://dx.doi.org/10.1038/nature05596

BoSmith, R.E., I. Briggs, and N.C. Sturgess. 1993. Inhibitory actions of ZENECA ZD7288 on whole-cell hyperpolarization activated inward current (If) in guinea-pig dissociated sinoatrial node cells. *Br. J. Pharmacol.* 110:343–349.

Chan, Y.C., K. Wang, K.W. Au, C.P. Lau, H.F. Tse, and R.A. Li. 2009. Probing the bradycardic drug binding receptor of HCN-encoded pacemaker channels. *Pflugers Arch.* 459:25–38. (published erratum appears in *Pflugers Arch.* 2010. 459:519) http://dx.doi.org/10.1007/s00424-009-0719-2

Changeux, J.P., and S.J. Edelstein. 2005. Allosteric mechanisms of signal transduction. *Science.* 308:1424–1428. http://dx.doi.org/10.1126/science.1108595

Chen, J., J.S. Mitcheson, M. Tristani-Firouzi, M. Lin, and M.C. Sanguinetti. 2001. The S4-S5 linker couples voltage sensing and activation of pacemaker channels. *Proc. Natl. Acad. Sci. USA.* 98:11277–11282. http://dx.doi.org/10.1073/pnas.201250598

Cheng, L., K. Kinard, R. Rajamani, and M.C. Sanguinetti. 2007. Molecular mapping of the binding site for a blocker of hyperpolarization-activated, cyclic nucleotide-modulated pacemaker channels. *J. Pharmacol. Exp. Ther.* 322:931–939. http://dx.doi.org/10.1124/jpet.107.121467

Craven, K.B., and W.N. Zagotta. 2004. Salt bridges and gating in the COOH-terminal region of HCN2 and CNGA1 channels. *J. Gen. Physiol.* 124:663–677. http://dx.doi.org/10.1085/jgp.200409178

Craven, K.B., and W.N. Zagotta. 2006. CNG and HCN channels: two peas, one pod. *Annu. Rev. Physiol.* 68:375–401. http://dx.doi.org/10.1146/annurev.physiol.68.040104.134728

Decher, N., J. Chen, and M.C. Sanguinetti. 2004. Voltage-dependent gating of hyperpolarization-activated, cyclic nucleotide-gated pacemaker channels: molecular coupling between the S4-S5 and C-linkers. *J. Biol. Chem.* 279:13859–13865. http://dx.doi.org/10.1074/jbc.M313704200

Denyer, J.C., and H.F. Brown. 1990. Pacemaking in rabbit isolated sino-atrial node cells during Cs+ block of the hyperpolarization-activated current if. *J. Physiol.* 429:401–409.

DiFrancesco, D. 1982. Block and activation of the pace-maker channel in calf purkinje fibres: effects of potassium, caesium and rubidium. *J. Physiol.* 329:485–507.

Fain, G.L., F.N. Quandt, B.L. Bastian, and H.M. Gerschenfeld. 1978. Contribution of a caesium-sensitive conductance increase to the rod photoresponse. *Nature.* 272:467–469. http://dx.doi.org/10.1038/272467a0

Flynn, G.E., K.D. Black, L.D. Islas, B. Sankaran, and W.N. Zagotta. 2007. Structure and rearrangements in the carboxy-terminal region of SpIH channels. *Structure.* 15:671–682. http://dx.doi.org/10.1016/j.str.2007.04.008

Hackos, D.H., T.H. Chang, and K.J. Swartz. 2002. Scanning the intracellular S6 activation gate in the shaker K^+ channel. *J. Gen. Physiol.* 119:521–532. http://dx.doi.org/10.1085/jgp.20028569

Harris, N.C., and A. Constanti. 1995. Mechanism of block by ZD 7288 of the hyperpolarization-activated inward rectifying current in guinea pig substantia nigra neurons in vitro. *J. Neurophysiol.* 74:2366–2378.

Henzler-Wildman, K.A., V. Thai, M. Lei, M. Ott, M. Wolf-Watz, T. Fenn, E. Pozharski, M.A. Wilson, G.A. Petsko, M. Karplus, et al. 2007. Intrinsic motions along an enzymatic reaction trajectory. *Nature.* 450:838–844. http://dx.doi.org/10.1038/nature06410

Hille, B. 2001. Ion Channels of Excitable Membranes. Third edition. Sinauer, Sunderland, MA. 814 pp.

Hua, L., and S.E. Gordon. 2005. Functional interactions between A' helices in the C-linker of open CNG channels. *J. Gen. Physiol.* 125:335–344. http://dx.doi.org/10.1085/jgp.200409187

Jan, L.Y., and Y.N. Jan. 1990. A superfamily of ion channels. *Nature.* 345:672. http://dx.doi.org/10.1038/345672a0

Kaupp, U.B., and R. Seifert. 2002. Cyclic nucleotide-gated ion channels. *Physiol. Rev.* 82:769–824.

Kusch, J., C. Biskup, S. Thon, E. Schulz, V. Nache, T. Zimmer, F. Schwede, and K. Benndorf. 2010. Interdependence of receptor activation and ligand binding in HCN2 pacemaker channels. *Neuron.* 67:75–85. http://dx.doi.org/10.1016/j.neuron.2010.05.022

Long, S.B., X. Tao, E.B. Campbell, and R. MacKinnon. 2007. Atomic structure of a voltage-dependent K+ channel in a lipid membrane-like environment. *Nature.* 450:376–382. http://dx.doi.org/10.1038/nature06265

Lopatin, A.N., E.N. Makhina, and C.G. Nichols. 1994. Potassium channel block by cytoplasmic polyamines as the mechanism of intrinsic rectification. *Nature.* 372:366–369. http://dx.doi.org/10.1038/372366a0

Lyashchenko, A.K., and G.R. Tibbs. 2008. Ion binding in the open HCN pacemaker channel pore: Fast mechanisms to shape "slow" channels. *J. Gen. Physiol.* 131:227–243. http://dx.doi.org/10.1085/jgp.200709868

Männikkö, R., F. Elinder, and H.P. Larsson. 2002. Voltage-sensing mechanism is conserved among ion channels gated by opposite voltages. *Nature.* 419:837–841. http://dx.doi.org/10.1038/nature01038

Monod, J., J. Wyman, and J.P. Changeux. 1965. On the nature of allosteric transitions: A plausible model. *J. Mol. Biol.* 12:88–118. http://dx.doi.org/10.1016/S0022-2836(65)80285-6

Paoletti, P., E.C. Young, and S.A. Siegelbaum. 1999. C-Linker of cyclic nucleotide–gated channels controls coupling of ligand binding to channel gating. *J. Gen. Physiol.* 113:17–34. http://dx.doi.org/10.1085/jgp.113.1.17

Prole, D.L., and G. Yellen. 2006. Reversal of HCN channel voltage dependence via bridging of the S4–S5 linker and Post-S6. *J. Gen. Physiol.* 128:273–282. http://dx.doi.org/10.1085/jgp.200609590

Richards, M.J., and S.E. Gordon. 2000. Cooperativity and cooperation in cyclic nucleotide-gated ion channels. *Biochemistry.* 39:14003–14011. http://dx.doi.org/10.1021/bi001639i

Robinson, R.B., and S.A. Siegelbaum. 2003. Hyperpolarization-activated cation currents: from molecules to physiological function. *Annu. Rev. Physiol.* 65:453–480. http://dx.doi.org/10.1146/annurev.physiol.65.092101.142734

Rosenbaum, T., and S.E. Gordon. 2004. Quickening the pace: looking into the heart of HCN channels. *Neuron.* 42:193–196. http://dx.doi.org/10.1016/S0896-6273(04)00199-0

Rothberg, B.S., K.S. Shin, P.S. Phale, and G. Yellen. 2002. Voltage-controlled gating at the intracellular entrance to a hyperpolarization-activated cation channel. *J. Gen. Physiol.* 119:83–91. http://dx.doi.org/10.1085/jgp.119.1.83

Rothberg, B.S., K.S. Shin, and G. Yellen. 2003. Movements near the gate of a hyperpolarization-activated cation channel. *J. Gen. Physiol.* 122:501–510. http://dx.doi.org/10.1085/jgp.200308928

Shin, K.S., C. Maertens, C. Proenza, B.S. Rothberg, and G. Yellen. 2004. Inactivation in HCN channels results from reclosure of the activation gate: desensitization to voltage. *Neuron.* 41:737–744. http://dx.doi.org/10.1016/S0896-6273(04)00083-2

Swartz, K.J. 2005. Structure and anticipatory movements of the S6 gate in K_v channels. *J. Gen. Physiol.* 126:413–417. http://dx.doi.org/10.1085/jgp.200509430

Ulens, C., and S.A. Siegelbaum. 2003. Regulation of hyperpolarization-activated HCN channels by cAMP through a gating switch in binding domain symmetry. *Neuron.* 40:959–970. http://dx.doi.org/10.1016/S0896-6273(03)00753-0

Vemana, S., S. Pandey, and H.P. Larsson. 2004. S4 movement in a mammalian HCN channel. *J. Gen. Physiol.* 123:21–32. http://dx.doi.org/10.1085/jgp.200308916

Vemana, S., S. Pandey, and H.P. Larsson. 2008. Intracellular Mg2+ is a voltage-dependent pore blocker of HCN channels. *Am. J. Physiol. Cell Physiol.* 295:C557–C565. http://dx.doi.org/10.1152/ajpcell.00154.2008

Wang, J., S. Chen, M.F. Nolan, and S.A. Siegelbaum. 2002. Activity-dependent regulation of HCN pacemaker channels by cyclic AMP: signaling through dynamic allosteric coupling. *Neuron.* 36:451–461. http://dx.doi.org/10.1016/S0896-6273(02)00968-6

Webster, S.M., D. Del Camino, J.P. Dekker, and G. Yellen. 2004. Intracellular gate opening in Shaker K+ channels defined by high-affinity metal bridges. *Nature.* 428:864–868. http://dx.doi.org/10.1038/nature02468

Wu, S., Z.V. Vysotskaya, X. Xu, C. Xie, Q. Liu, and L. Zhou. 2011. State-dependent cAMP binding to functioning HCN channels studied by patch-clamp fluorometry. *Biophys. J.* 100:1226–1232. http://dx.doi.org/10.1016/j.bpj.2011.01.034

Xu, X., Z.V. Vysotskaya, Q. Liu, and L. Zhou. 2010. Structural basis for the cAMP-dependent gating in the human HCN4 channel. *J. Biol. Chem.* 285:37082–37091. http://dx.doi.org/10.1074/jbc.M110.152033

Yang, J., Y.N. Jan, and L.Y. Jan. 1995. Control of rectification and permeation by residues in two distinct domains in an inward rectifier K+ channel. *Neuron.* 14:1047–1054. http://dx.doi.org/10.1016/0896-6273(95)90343-7

Zagotta, W.N., and S.A. Siegelbaum. 1996. Structure and function of cyclic nucleotide-gated channels. *Annu. Rev. Neurosci.* 19:235–263. http://dx.doi.org/10.1146/annurev.ne.19.030196.001315

Zagotta, W.N., N.B. Olivier, K.D. Black, E.C. Young, R. Olson, and E. Gouaux. 2003. Structural basis for modulation and agonist specificity of HCN pacemaker channels. *Nature.* 425:200–205. http://dx.doi.org/10.1038/nature01922

Zhou, L., and S.A. Siegelbaum. 2007. Gating of HCN channels by cyclic nucleotides: residue contacts that underlie ligand binding, selectivity, and efficacy. *Structure.* 15:655–670. http://dx.doi.org/10.1016/j.str.2007.04.012

Zhou, L., N.B. Olivier, H. Yao, E.C. Young, and S.A. Siegelbaum. 2004. A conserved tripeptide in CNG and HCN channels regulates ligand gating by controlling C-terminal oligomerization. *Neuron.* 44:823–834. http://dx.doi.org/10.1016/j.neuron.2004.11.012

Zong, X., H. Zucker, F. Hofmann, and M. Biel. 1998. Three amino acids in the C-linker are major determinants of gating in cyclic nucleotide-gated channels. *EMBO J.* 17:353–362. http://dx.doi.org/10.1093/emboj/17.2.353